Laser-Beam Deflection Induced by Transverse Plasma Flow

D. E. Hinkel

E. A. Williams

C. H. Still

Introduction

Recent experiments[1,2] conducted at Lawrence Livermore National Laboratory (LLNL) using the Nova laser show anomalous deflections of the laser beam in the plasma. In gas-filled hohlraum experiments,[1] the laser spot on the hohlraum wall is 100–150 μm closer to the laser entrance hole (LEH) than in empty hohlraum experiments. This corresponds to a beam deflection of roughly 6° if the deflection occurs near the LEH. In a series of exploding foil experiments,[2] intensity-dependent deflection of a transmitted probe beam is observed.

Simulations by the hydro code LASNEX,[1,3] which accurately model empty hohlraum experiments, do not show beam deflection in gas-filled hohlraums. Neither whole-beam refraction nor differential laser absorption accounts for the experimental results (because the laser makes an angle of 50° with the hohlraum axis, the path length of the innermost portion of the laser beam is longer than that of the outermost portion). In this article, we show that, in the hohlraum plasma, effects of flow transverse to the laser propagation direction on (1) filamentation and (2) forward Brillouin scatter (FBS) can account for this anomalous deflection.

Model for Transverse-Flow–Induced Beam Deflection

Solution of the steady-state filamentation dispersion relation shows that filaments grow in a direction tilted downstream to the initial beam direction.[4] This mechanism was recently proposed[5] as a cause of beam deflection in the aforementioned hohlraum experiments.

In this article, we examine a group of related mechanisms for laser beam deflection. In the presence of a transverse plasma flow, ponderomotively (or thermally) created density depressions form *downstream* from the laser beam's high-intensity regions. Light refracted into the lowered density is thus deflected in the direction of the flow. We use the numerical model F3D to quantify these mechanisms.[6] To illustrate the physics, a highly simplified, steady-state model is used,

$$\left(2ik_0\frac{\partial}{\partial z}+\nabla_\perp^2\right)\psi=-\frac{\omega_{pe}^2}{c^2}\delta n\,\psi \qquad (1a)$$

$$\left[M\frac{\partial}{\partial x}\left(M\frac{\partial}{\partial x}+\kappa\right)-\nabla_\perp^2\right]\delta n=\left(\frac{v_0}{v_e}\right)^2\nabla_\perp^2|\psi|^2 \quad . \qquad (1b)$$

Equation (1a) describes the light wave amplitude ψ (vector potential scaled to its mean value) in the paraxial approximation, scattered by the fractional density perturbations δn. Equation (1b) gives the steady-state density response to the ponderomotive force. In these equations, the light is propagating in the $\mathbf{e}_z$ direction, and the density fluctuations propagate only in the transverse direction. Here, k_0 is the vacuum wave number, n_0 is the unperturbed plasma density, ω_{pe} is the electron plasma frequency, and c is the speed of light. Also, $M \equiv u/C_s$ is the Mach number of the flow u in the x direction, with C_s the sound speed, κ the spatial damping rate of ion acoustic waves, v_0 the quiver velocity of an electron in the mean light wave field, and v_e the electron thermal velocity. The density response calculated by F3D in steady state,[6] when thermal effects are neglected, is that given by Eq. (1b). In highly collisional plasmas, thermal effects supplement the ponderomotive potential, thereby increasing filamentation, and might be expected to similarly increase deflection.

Equations of motions for the beam centroid and width can be derived by taking intensity-weighted moments of Eq. (1a). Defining

$$\langle \mathbf{x} \rangle \equiv \int \psi^* \mathbf{x}\, \psi\, d^2x \;, \quad \langle \mathbf{k} \rangle \equiv -i \int \psi^* \nabla \psi\, d^2x$$

etc., we obtain

$$\frac{\partial^2}{\partial z^2}\langle \mathbf{x} \rangle = -\frac{\omega_{pe}^2}{2k_0^2 c^2}\langle \nabla \delta n \rangle, \tag{2a}$$

$$\frac{\partial^2}{\partial z^2}\left\langle \left(\mathbf{x} - \langle \mathbf{x} \rangle\right)^2 \right\rangle = \frac{2}{k_0^2} \times \left[\left\langle \left(\mathbf{k} - \langle \mathbf{k} \rangle\right)^2 \right\rangle - \frac{\omega_{pe}^2}{c^2} \left\langle \left(\mathbf{x} - \langle \mathbf{x} \rangle\right) \left(\nabla \delta n \right) \right\rangle \right]. \tag{2b}$$

Equation (2b) is analogous to Eq. (11) of Ref. [7]. Similar equations have also been derived in Refs. [8] and [9].

In Eq. (2a), the transverse density gradient refracts the light toward regions of lower electron density. In Eq. (2b), the beam width is determined by the competition between diffraction [first term on right-hand side (RHS) of Eq. (2b)] and self-focusing [second term on RHS of Eq. (2b)].

When the Fourier transform of Eq. (1b) is substituted into Eq. (2a),

$$\frac{\partial^2 \langle \mathbf{x} \rangle}{\partial z^2} = -\frac{i\omega_{pe}^2 v_0^2}{2k_0^2 c^2 v_e^2} \times \int \frac{d^2k \left|\tilde{\psi}(k)\right|^2 \left|\tilde{\psi}(-k)\right|^2 k^2 \mathbf{k}}{k_x^2\left(M^2 - 1\right) - i\bar{\kappa} M k \left(k_x - k_y^2\right)}, \tag{3}$$

where we have defined the wave amplitude damping decrement $\bar{\kappa} \equiv \kappa/k$. (Setting $\bar{\kappa}$ = constant approximately represents Landau damping.) The y component of the above equation yields $\partial y/\partial z^2 = 0$, as the integrand is an odd function of k_y. In the absence of flow, then, the beam is not deflected.

In the x direction, for subsonic flow ($M < 1$), only the even portion of the integrand survives, and the deflection can be seen to be an increasing function of M, and to be proportional to the damping decrement. The deflection (i.e., $\partial^2 x/\partial z^2$) is greatest for two-dimensional (2D) perturbations with $k_y = 0$, where the denominator is smallest.

In a non-steady-state model, there would have been an additional transient density response over a characteristic time scale $t = a/(1 - M)C_s$, where a is the beam width, even when $\kappa = 0$. This is most significant as $M \to 1$, when the ion acoustic damping is weak.

With supersonic transverse flow ($M > 1$), the integrand in Eq. (3) has a resonant contribution where

$$k_y = k_x \sqrt{M^2 - 1}.$$

This is the matching condition for forward SBS, where different k components of the beam are coupled by ion acoustic waves Doppler shifted to zero frequency. In 2D, the resonance occurs only at $M = 1$.

Substitution of the Fourier transform of δn as determined from Eq. (1b) into the second term on RHS of Eq. (2b) shows that the self-focusing of the beam is proportional to

$$\partial_{k_x}\left\{ k_x k^2 / \left[k_x^2\left(1 - M^2\right) + k_y^2 \right] \right\}.$$

This expression is always positive definite for M<1, and increases the self-focusing in the flow direction over that experienced by the beam in the nonflow direction.

Numerical Simulations of the Ponderomotive Density Response

We examined the density response of a transversely flowing plasma to a legislated Gaussian laser wave amplitude $\psi = \exp[-(x^2 + y^2)/2\sigma^2]$. We compared the linearized response obtained analytically from Eq. (1b) (with time dependence retained, but with zero damping)[10] to the nonlinear response computed numerically using the Eulerian, 3D hydrodynamics code NH3,[11] in which the plasma is treated as a single, nondissipative, nonconducting fluid. For example, when $M = 1.2$, a ponderomotive potential that drives a maximum linearized density response of $\delta n \sim 25\%$ has a corresponding nonlinear response approximately 20% smaller. However, there is only a 2.5% difference between δn_{lin} and δn_{nl} i.e., in the centroid deflection as governed by Eq. (2a). Since such large density perturbations are reached only in very localized regions of plasma, we do

not anticipate that the results presented here would be modified by the inclusion of nonlinearity. For more strongly driven systems, this may not be the case.[12]

2D Simulations of a Gaussian Beam

Motivated by the above considerations, we performed a series of 2D and 3D F3D simulations.[6] The plasma parameters chosen are characteristic of LASNEX simulations[1,3] of gas-filled hohlraums near the sonic point in the transverse flow, where the plasma electron density is $n = 0.1n_c$, n_c being the critical density, and the electron temperature is $T_e = 3$ keV. We initially modeled a single hot spot of the Nova beam (a hot spot is a portion of the beam that is more intense; this region of higher intensity is caused by constructive interference between coherent pieces of the beam). In these 2D simulations, the incident laser amplitude is Gaussian with peak intensity $\bar{I}$ and beam width variance $\sigma^2 = a^2$, corresponding to an input wave field $\psi = (x,z = 0) = \exp(-x^2/2a^2)$.

Simulations in 2D with a constant transverse flow and zero damping decrement (but with time dependence retained) were performed where the laser intensity and system length varied. The amount of beam deflection increases approximately linearly with laser intensity (for $1 \times 10^{15} \le \bar{I} \le 6 \times 10^{15}$ W/cm^2) and system length (for $0 \le L \le 1000\lambda_0$). By varying the width of the Gaussian beam ($2\lambda_0 \le a \le 100\lambda_0$), we found that maximum filamentation amplication and beam deflection occurs for $a \approx 10\lambda_0$, corresponding to the peak linear gain rate (without flow) [$\kappa_{fil} = 0.125(v_0/v_e)^2(n/n_c)$ for $a^{-1} = 0.5k_0(v_0/v_e)(n/n_c)^{1/2}$].

LASNEX simulations[1,3] of gas-filled hohlraums indicate that the plasma flow transverse to the laser beam is sheared, i.e., $\mathbf{u} \approx u_0(1 + z/L_v)\mathbf{e}$, with $L_v \approx 500$ μm, and that the transverse flow profile has a sonic point on a long shelf of plasma with density $n = 0.1n_c$. The laser propagation was simulated in the vicinity of the transverse sonic point; i.e., M decreased linearly from a value of 1.1 at $z = 0$ to a value of 0.5 at $z = 1000\lambda_0$, where $\lambda_0 = 0.351$ μm. Figure 1 is a surface plot of the laser intensity with $\bar{I} = 6 \times 10^{15}$ W/cm^2 and $a = 10\lambda_0$ at time $t = 90$ ps. These values of peak intensity and beam width mimic the peak intensity and transverse size of laser hot spots 1 mm beyond best focus for an unsmoothed Nova beam,[13] i.e., near the LEH. The entrance plane ($z = 0$) is at the top of the figure. In this plane, the beam is centered in the middle of the box. At $z = 1000\lambda_0$, the beam is no longer centered. Approximately 70% of the beam energy is deflected

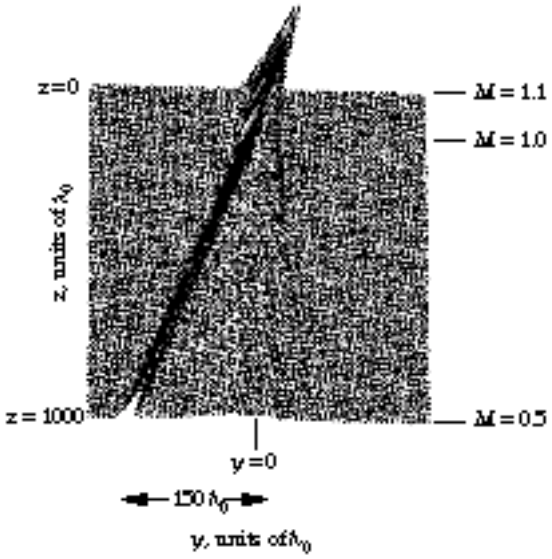

FIGURE 1. A surface plot of the laser intensity of a 2D Gaussian beam at time t =90ps for $\bar{I} = 6 \times 10^{15}$ W/cm^2, $n = 0.1n_c$, $T_e = 3$ keV, $\bar{v} = 0$, and transverse flow scale length $L = 500$ μm. The initial beam width is $a = 10\lambda_0$, where $\lambda_0 = 0.351$ μm. Approximately 70% of the beam deflects 9°, and self-focuses as well. The remainder of the beam not captured in the filament travels undeflected through the system. (08-00-0697-1094pb01)

in the direction of the flow in the vicinity of the transverse sonic point, at $z = 150\lambda_0$, and the remainder of the beam is undeflected and is also defocused by diffraction.

3D Simulations of an RPP Beam

The 2D simulation described above illustrates the deflection of one hot spot. Near the focal plane, the beam consists of many spots of varying power and size. To model the laser beam more accurately, we performed simulations in 3D with a model of the laser beam at best focus when random phase plates (RPP) are used.[14] The RPP technique produces a large number of beamlets in the laser beam with random phases. The superposition of these beamlets yields spikes (from constructive interference) and depressions (from destructive interference) in the intensity pattern, i.e., speckles. A speckle length is typically $L_s \equiv 8f^2\lambda_0$, where f is the f number of the lens.

We simulated a piece of the RPP Nova beam near peak intensity, where $I_0 = 3 \times 10^{15}$ W/cm^2 in $f/4$ focusing geometry. All other plasma parameters were unchanged, except the damping decrement, $\bar{\kappa} \equiv v/kC_s = 0.1$. Figure 2 depicts the effect of transverse flow on the hot spots of the laser beam. Plotted are contours of laser intensity greater than or equal to $5I_0$. The laser

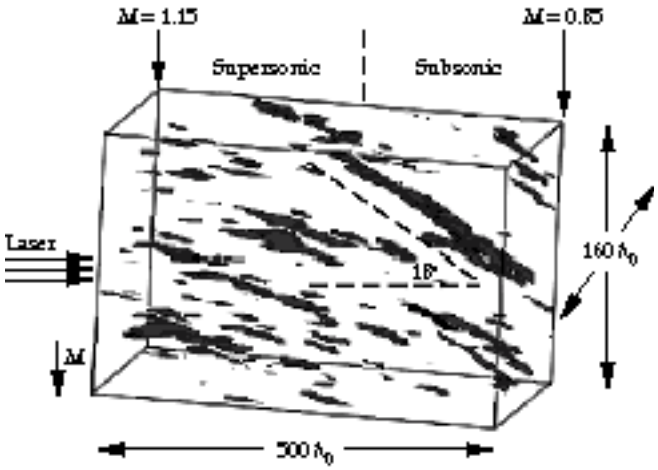

FIGURE 2. A plot of the hot spots of a 3D, RPP laser beam at time $t = 90$ ps for $\bar{I}_0 = 3 \times 10^{15}$ W/cm^2, $n/n_c = 0.1$, $T_e = 3$ keV, $\bar{\kappa} = 0.1$, and transverse flow scale length $L_v = 500$ μm. The speckle length is $L_s = 128\lambda_0$, where $\lambda_0 = 0.351$ μm. Those portions of the laser beam at intensities greater than or equal to $5I_0$ are shown. The hot spots of the laser beam undergo deflection of 18°; the calculated centroid of the beam deflects 6°. In the subsonic region, the hot spots also show evidence of self-focusing. (08-00-0697-1095pb01)

beam enters from the left side of the simulation box, where the downwardly directed transverse flow decreases linearly from $M = 1.15$ to $M = 0.85$ on the right side of the simulation box, with the transverse sonic point located at the center. In contrast to 2D simulations, where deflection is localized at the sonic point, in 3D, beam deflection occurs throughout the supersonic region, where internal FBS between different k components of the beam takes place.

In the subsonic region, the hot spots become wider, indicating that the area of the beam at intensities greater than or equal to $5I_0$ has increased. The beam hot spots are undergoing self-focusing in addition to deflection. The calculated centroid of the laser beam has deflected by 6° at the exit plane, roughly 1/3 of the deflection of the intense parts of the beam (18°) shown in Figure 2.

A series of 3D RPP simulations was also performed at the above parameters to determine the Mach number scaling. The constant (over the simulation system) transverse flow was increased from $M = 0$ to $M = 1$ in successive simulations, and we found that the deflection approximately scales as $M/(2 - M^2)^2$. This is in agreement with Eq. (3), where, for a circular beam ($k_x \approx k_y$), the calculated deflection is proportional to $M/(2 - M^2)^2$.

We also performed 3D simulations incorporating smoothing by spectral dispersion (SSD),[15] which causes the speckles to move around and appear or disappear as a function of time. (At any given instant, an SSD beam has a sinusoidal variation in frequency with transverse wave number.) SSD is most effective when there is at least one complete color cycle of the sinusoid. Application of 3 Å of bandwidth to a laser beam dispersed by a grating that provides 1.2 color cycles reduces deflection of the previously described RPP beam from 6° to roughly 2°. Figure 3 is a plot of the hot spots of the laser beam of Figure 2 when SSD with 3 Å of bandwidth is applied.

However, with sufficient bandwidth and dispersion, SSD can *induce* oscillatory (in time) beam deflection, even in the absence of flow. (In a time-averaged sense, i.e., when averaged over many SSD cycles, this deflection approaches zero.) Those k components of the beam that instantaneously have higher frequencies transfer energy to others at lower frequencies when the frequency and wave vector matching conditions for FBS are satisfied. This is the same physical mechanism believed to be responsible for the energy transfer between *separate* beams of different frequency, observed in experiments at LLNL.[16,17]

Figure 3 depicts the laser beam when the downstream edge of the beam is red, i.e., at the time when SSD is adding its maximum contribution to the beam deflection. Comparing Figure 3 to Figure 2, we see clearly that the amount of energy greater than or equal to $5I_0$ is reduced for the SSD beam (i.e., self-focusing is reduced) and that the amount of deflection of the hot spots is greatly reduced as well (18° in Figure 2 vs 5° in Figure 3). In simulations without flow, but with 3 Å of bandwidth applied to an SSD beam, the beam

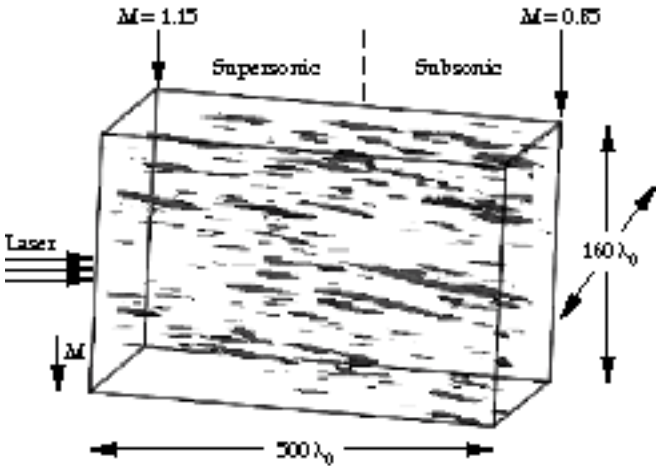

FIGURE 3. A plot of the hot spots of a 3D, RPP laser beam with SSD and 3 Å of bandwidth at time $t = 90$ ps for $\bar{I}_0 = 3 \times 10^{15}$ W/cm^2, $n/n_c = 0.1$, $T_e = 3$ keV, $\bar{\kappa} = 0.1$, and transverse flow scale length $L_v = 500$ μm. The speckle length is $L_s = 128\lambda_0$, where $\lambda_0 = 0.351$ μm. Those portions of the laser beam at intensities greater than or equal to $5I_0$ are shown. The centroid of the beam deflects by 2° at the exit plane, and the hot spots are deflected about 5°. There is less deflection and self-focusing than in Figure 2. (08-00-0697-1096pb01)

centroid deflection (which is caused by the SSD itself) is roughly 2° at the time when the downstream edge of the beam is red (time of maximum deflection). Thus, in Figure 3, the deflection is primarily caused by the SSD itself, and not by the flow.

In a 2D, steady-state model, the linearized density response diverges as $M \rightarrow 1$. This divergence is mitigated by inclusion of 3D effects and/or ion wave damping when $\kappa a > 1 - M$, where a is the beam width. In the absence of these effects, fluid nonlinearity limits the resonance when $v_0/v_e > 1 - M$.[18] Nonlinear hydrodynamic effects become more significant at higher intensities than considered here, e.g., when $\delta n \rightarrow 1$. In the very near future, this problem will be examined at higher intensity, where the nonlinear aspects of this problem are important, via the incorporation of the nonlinear hydrodynamics package NH3 into F3D.

Summary

Recent experiments in gas-filled hohlraums suggest that laser beams refract more than calculated by the hydrocode LASNEX. We show, from theoretical arguments and three-dimensional simulations with F3D, that transverse plasma flow causes a deflection in the inferred direction of the appropriate magnitude. The physical mechanisms involve filamentation and forward SBS. In each case, the density depressions created by the laser's ponderomotive force are swept downstream by the transverse flow. The displaced depressions then refract the laser energy in the direction of the flow.

Acknowledgments

We acknowledge invaluable input from R. L. Berger, L. V. Powers, T. W. Johnston, B. B. Afeyan, D. Dubois, S. G. Glendinning, R. L. Kauffman, W. L. Kruer, A. B. Langdon, J. D. Moody, and H. A. Rose.

Notes and References

1. S. G. Glendinning, private communication.
2. J. D. Moody et al., *Phys. Rev. Lett.* **77**, 1294 (1996).
3. G. Zimmerman and W. L. Kruer, *Comments Plasma Phys. Controlled Fusion* **2**, 85 (1975).
4. R. W. Short, R. Bingham, and E. A. Williams, *Phys. Fluids* **25**, 2302 (1982).
5. H. A. Rose, *Phys. Plasmas* **3**, 1709 (1996).
6. R. L. Berger et al., *Phys. FluidsB* **5**, 2243 (1993).
7. C. E. Max, *Phys. Fluids* **19,** 74 (1976).
8. M. V. Goldman, K. Rypdal, and B. Hafizi, *Phys. Fluids* **23**, 945 (1980).
9. J. J. Rasmussen and K. Rypdal, *Phys. Scr*. **33**, 481 (1986).
10. E. A. Williams and D. E. Hinkel, *Bull. Am. Phys. Soc.* **40**, 1824 (1995).
11. C. H. Still et al., *Bull. Am. Phys. Soc*. **40**, 1823 (1995).
12. In F3D there is an imposed saturation of the density perturbations, using $\log(l + \delta n)$ in lieu of δn as the linearized density variable. This prevents the nonphysical singularities of the nonlinear Schrödinger equation (NLSE), Eq. (1a), which can occur at higher intensities than used in these simulations. For the F3D simulation results presented in this article, the imposed saturation had negligible effect.
13. P. Wegner, "Measurements and Modeling of Laser Irradiance in the High-Power Third Harmonic Nova Focus," Lawrence Livermore National Laboratory, Livermore, CA, UCRL-ID-110480 (1992).
14. Y. Kato et al., *Phys. Rev. Lett.* **53**, 1057 (1984).
15. S. Skupsky et al., *J. Appl. Phys*. **66**, 3456 (1989).
16. W. L. Kruer et al., *Phys. Plasmas* **3**, 382 (1996).
17. R. K. Kirkwood et al., *Phys. Rev. Lett.* **76**, 2065 (1996).
18. W. L. Kruer and J. H. Hammer, *Comments Plasma Phys. Controlled Fusion* **18**, 85 (1997).